9-1-2020

Quantification and characterization of granulocyte macrophage colony-stimulating factor activated human peripheral blood mononuclear cells by fluorine-19 cellular MRI in an immunocompromised mouse model

C Fink

M Smith

O C Sehl

J M Gaudet

T C Meagher

See next page for additional authors

Authors

C Fink, M Smith, O C Sehl, J M Gaudet, T C Meagher, N A Sheikh, Jimmy Dikeakos, Michael Rieder, P J Foster, and G A Dekaban

Diagnostic and Interventional Imaging (2020) **101**, 577—588

ORIGINAL ARTICLE / *Cancer imaging*

Quantification and characterization of granulocyte macrophage colony-stimulating factor activated human peripheral blood mononuclear cells by fluorine-19 cellular MRI in an immunocompromised mouse model

C. Fink[a,c], M. Smith[a,c], O.C. Sehl[b,d], J.M. Gaudet[b,d,1], T.C. Meagher[f,2], N.A. Sheikh[f], J.D. Dikeakos[c], M.J. Rieder[a,e], P.J. Foster[b,d], G.A. Dekaban[a,c,*]

[a] *Biotherapeutics Research Laboratory, Robarts Research Institute, London, Ontario N6A 5B7, Canada*
[b] *Imaging Research Laboratories, Robarts Research Institute, London, Ontario N6A 5B7, Canada*
[c] *Department of Microbiology and Immunology, University of Western Ontario, London, Ontario N6A 5B7, Canada*
[d] *Department of Medical Biophysics, University of Western Ontario, London, Ontario N6A 5B7, Canada*
[e] *Department of Pediatrics, University of Western Ontario, London, Ontario N6A 5B7, Canada*
[f] *Dendreon Corporation, Seattle, Washington 98102, USA*

KEYWORDS
Antigen presenting cell (APC) ;
Fluorine-19 (19F) ;
Cellular magnetic resonance imaging (MRI) ;
Cancer immunotherapy

Abstract
Purpose. — The purpose of this study was to test fluorine-19 (19F) cellular magnetic resonance (MRI) as a non-invasive imaging modality to track therapeutic cell migration as a surrogate marker of immunotherapeutic effectiveness.
Materials and methods. — Human peripheral blood mononuclear cell- (PBMC)-derived antigen presenting cell (APC) were labeled with a 19F-perfluorocarbon (PFC) and/or activated with granulocyte macrophage colony-stimulating factor (GM-CSF). Viability, phenotype and cell lineage characterization preceded 19F cellular MRI of PFC$^+$ PBMC under both pre-clinical 9.4 Tesla (T) and clinical 3T conditions in a mouse model.

* Corresponding author. Robarts Research Institute, 1151 Richmond Street North, London, Ontario, N6A 5B7, Canada.
Adresse e-mail : dekaban@robarts.ca (G.A. Dekaban).
[1] Present address: Magnetic Insight, Inc., Alameda, California 94501, USA.
[2] Present address: Regeneron Pharmaceuticals, Inc., Tarrytown, New York 10591, USA.

https://doi.org/10.1016/j.diii.2020.02.004

Results. — A high proportion of PBMC incorporated PFC without affecting viability, phenotype or cell lineage composition. PFC^+ PBMC were *in vivo* migration-competent to draining and downstream lymph nodes. GM-CSF addition to culture increased PBMC migration to, and persistence within, secondary lymphoid organs.
Conclusion. — 19F cellular MRI is a non-invasive imaging technique capable of detecting and quantifying *in vivo* cell migration in conjunction with an established APC-based immunotherapy model. 19F cellular MRI can function as a surrogate marker for assessing and improving upon the therapeutic benefit that this immunotherapy provides.

Introduction

The *ex vivo* generation of antigen presenting cell- (APC)-based cancer immunotherapies is a leading strategy to avoid and combat tumor-induced immune suppression that prevents effective anti-tumor immune responses from being launched [1—3]. Originally, dendritic cells (DC) were employed as professional APC because they induce potent *de novo* tumor-associated antigen-(TAA)-specific immune responses [4]. Due to their *in vivo* scarcity, DC can be differentiated *ex vivo* from monocytes co-cultured with differentiation-inducing growth factors such as granulocyte macrophage colony-stimulating factor (GM-CSF) [3,5]. Lengthy *ex vivo* culture is often required to produce monocyte-derived DC (moDC)-based immunotherapies but can also promote tolerogenic TAA-specific immune responses upon autologous adoptive transfer [6,7].

To reduce extensive *ex vivo* culture, peripheral blood mononuclear cells (PBMC) have served as precursors for APC-based immunotherapies. An example is Sipuleucel-T (Provenge®), which is a cell-based vaccine for the treatment of metastatic castration-resistant prostate cancer (mCRPC) manufactured by culturing PBMC *ex vivo* with GM-CSF linked to the TAA, prostatic acid phosphatase (PAP) [8]. GM-CSF is central to immunotherapeutic effectiveness as it up-regulates markers of activation, migration, co-stimulation and antigen presentation on APC [4,9,10]. Specifically, CD54 present on activated APC stabilizes the immunological synapse between APC and antigen-specific $CD4^+/CD8^+$ T cells in secondary lymphoid organs to induce an effective TAA-specific immune response [9,11]. Despite GM-CSF activation, a phase III clinical trial (NCT00065442) reported that Provenge® only prolonged overall survival of mCRPC patients by 4.1 months [12]. This is similar to the survival benefit reported for other mCRPC treatment regimens [13] yet clearly highlights the urgent need to improve mCRPC immunotherapeutics.

With APC-based immunotherapies, migration to secondary lymphoid organs is not only essential but is predictive of the magnitude of the ensuing immune response as well [14—16]. Cellular MRI that detects both fluorine-19 (19F) and anatomical/hydrogen-1 (1H) signal is capable of quantitatively tracking human and mouse 19F-perfluorocarbon (PFC)-labeled cells *in vivo* with high specificity [17—20]. We have also reported the *in vivo* detection of PFC^+, but otherwise unmanipulated, human PBMC migration to draining lymph nodes (LN) by both 9.4 Tesla (T) pre-clinical and 3T clinical MRI scanners [21].

The pre-clinical characterization of therapeutic APC formulations, including the effect of cytokine addition to *ex vivo* cultures and suitability of PFC as a cell tracking agent, are critical when considering clinical implementation. Due to the heterogenous composition of PBMC, the unique immunotherapeutic role of each cell lineage must also be preserved [22]. We expand on our previous studies to describe *in vivo* PFC^+ PBMC migration and persistence on a cell lineage basis in an effort to identify the role of GM-CSF-induced activation on *in vivo* PBMC fate and its possible association with immunotherapeutic potency.

The purpose of this study was to test 19F cellular MRI as a non-invasive imaging modality to track therapeutic cell migration as a surrogate marker of immunotherapeutic effectiveness.

Materials and methods

Animal care

Immunocompromised male NU/NU mice (Crl:NU-*Foxn1*^{NU}) were purchased from Charles River Laboratories (Saint Constant, CAN). All applicable institutional and/or national guidelines for the care and use of animals were followed.

Participants

The University of Western Ontario Health Sciences Research Ethics Board (REB Protocol #104593) pre-approved this protocol. Each participant aged 18 years or older provided a signed letter of informed consent prior to peripheral blood procurement and were self-reported free of human immunodeficiency virus, hepatitis B and C virus and other transmissible diseases. Commercially available PBMC products were also obtained from Stemcell Technologies (Seattle, USA). The complete reagent list is organized in Supplemental Table 1.

PBMC isolation and PFC labeling

The compatibility of GM-CSF addition to culture was tested with a previously optimized protocol for generating PFC$^+$ PBMC [21]. Briefly, peripheral blood or leukapheresis product was diluted with Hank's balanced salt solution and underwent density gradient centrifugation (Lymphoprep™) to isolate PBMC. PBMC were resuspended in AIM V® Medium CTS™ media (5×10^6 cells/mL) and labeled with PFC (5.0 mg/mL) or remained unlabeled (UL) for the first 24 hours of culture at 37 °C, 5% CO_2, and co-cultured ± GM-CSF (20 ng/mL) for the final 24 hours of a total 48 hour culture.

Alternatively, PBMC underwent negative magnetic selection using manufacturer's instructions to enrich for T cells, B cells and monocytes. Enriched cell cultures were resuspended in AIM V® Medium CTS™ media (± PFC) for 24 hours followed by GM-CSF addition for 24 hours further in Nunclon™ Sphera™ low attachment plates (Thermo Fisher Scientific).

Select PBMC samples were cryopreserved for long-term storage. Cryopreserved PBMC were cultured as outlined above to generate GM-CSF-treated PFC$^+$ or UL PBMC, with the only modification being overnight (~18 hours) rather than 48-hour culture.

PBMC viability

PBMC viability was measured using Trypan blue exclusion. To more stringently determine the effect of GM-CSF and PFC on the viability of both bulk PBMC and enriched cell lineages, LIVE/DEAD™ fixable aqua dead cell stain was used as described [21] and data was acquired with a LSRII analytical flow cytometer (BD Biosciences).

Flow cytometry

The fluorescent antibodies listed in Supplemental Table 1 were used for phenotyping following an aforementioned protocol [21]. For experiments pertaining to homogeneous cell lineage culturing (± PFC), T cells were labeled with CellTrace™ Far Red (Far Red), B cells with CellTrace™ Violet (CTV) and monocytes with CellTrace™ Carboxyfluorescein succinimidyl ester (CFSE) membrane-intercalating dyes (all 1 μM) following a previously detailed protocol [21]. Cell lineage enrichment and fluorescent label incorporation was verified by comparison to a cell aliquot removed before *in vitro* processing. All data was acquired using a BD Biosciences LSRII analytical flow cytometer.

Adoptive transfer of PBMC

The *in vivo* migration of GM-CSF-treated PFC$^+$ PBMC compared to untreated PFC$^+$ PBMC was assessed using 19F MRI. Three hours prior to PFC$^+$ PBMC administration, mouse interleukin-1β (IL-1β, 300 ng) was injected into the left popliteal LN (pLN) area of ($n = 4$) mice per donor PBMC to improve *in vivo* migration [15,23]. Two mice received hind footpad injections of 3×10^6 GM-CSF-treated PFC$^+$ PBMC while two different mice received 3×10^6 PFC$^+$ PBMC injections per PBMC product ($n = 4$). Injections were formulated in 40 μL phosphate-buffered saline.

Table 1 Clinical 3T 1H/19F MR imaging parameters.

Parameters	1H	19F
TR (ms)	12.8	5.8
TE (ms)	6.4	2.9
BW (kHz)	31.25	10
FA (°)	20	72
PC	6	1
NEX	1	200
FOV (mm^2)	60×30	60×30
Slice thickness (mm)	0.2	1
Matrix size (pixel)	300×150	60×30
Acquisition time (min)	25	35

TR: repetition time; TE: echo time; BW: bandwidth; FA: flip angle; PC: phase cycles; NEX: number of excitations; FOV: field of view.

Fluorescent mono-lineage cells were recombined at donor-specific physiologic proportions ($n = 3$) to formulate 3×10^6 PFC$^+$ and 3×10^6 UL PBMC injections into the right and left hind footpads, respectively, of ($n = 4$–5) mice. Separately, 3×10^6 PFC$^+$ PBMC and control UL PBMC from ($n = 3$) donors were injected into one hind and contralateral hind footpad, respectively, of ($n = 3$) mice/donor.

In a final adoptive transfer experiment, 3×10^6 and 6×10^6 PFC$^+$ GM-CSF-treated PBMC ($n = 3$ cryopreserved PBMC) were injected into the right hind and left hind footpads, respectively, of ($n = 2$–3) mice/donor. All mice were housed for two days after injection to permit *in vivo* PBMC migration.

MRI and quantification of PFC$^+$ PBMC migration

Imaging was performed two days after adoptive transfer on a 9.4T small animal MRI scanner (Varian) using identical 1H/19F imaging parameters outlined by our group [21]. Mice that received cryopreserved PFC$^+$ PBMC underwent 1H/19F MRI at both 24 and 48 hours post injection on a 3T clinical MRI scanner (Discovery® MR750, General Electric Healthcare) that employed a dual-tuned radiofrequency surface coil (Clinical MR Solutions) and a 3D-balanced steady state free precession sequence. MR acquisition parameters are presented in Table 1 and overlaid 1H/19F composite images (Osirix, Pixmeo SARL) provide anatomical reference. Voxel Tracker™ software (Celsense, Inc.) quantified *in vivo* 19F signal relative to reference tube signals containing a known amount of 19F spins (3.33×10^{16} 19F spins/μL) [24,25]. The mean signal-to-noise (SNR) ratio of LNs with detectable 19F signal was 7.37 (range: 5.36–10.12) at 3T.

Post-MRI verification of *in vivo* 19F signal

Following MRI completion, pLNs from mice that received triple-fluorescent PBMC (± PFC) were processed for digital fluorescence imaging as previously described [19]. Alternatively, pLNs from mice that received 3×10^6 non-fluorescent PBMC (± PFC) injections were processed into single cell

suspensions and surface stained for human CD45, CD3, CD20 and CD14 as stated above. Inguinal LN (iLN) single cell suspensions served as negative controls.

Statistical analysis

Quantitative variables were expressed as means ± SD and ranges. A paired *t*-test or ANOVA including multiple comparisons with Bonferroni *post-hoc* test (Graph Pad Prism 8) were used and was defined when statistics were reported. Significance was set at $P \leq 0.05$.

Results

GM-CSF promotes APC activation phenotype without affecting viability or PFC loading

GM-CSF (20 ng/mL) addition to cell cultures did not affect PFC$^+$ PBMC viability (85.7 ± 4.6 [SD] %; range: 79.3—90.4%) when compared to the PBMC viability cultured without GM-CSF (88.7 ± 3.7 [SD] %; range: 85.4—93.8%) ($P = 0.42$) (Fig. 1A). Similarly, GM-CSF did not significantly alter intraparticipant PFC uptake as ascertained using NMR spectroscopy (2.27 ± 1.87 [SD] × 10^{11} 19F spins/cell [range: 0.253—3.95 × 10^{11} 19F spins/cell]) versus (2.17 ± 1.60 [SD] × 10^{11} 19F spins/cell [range: 0.633—3.83 × 10^{11} 19F spins/cell]) in the presence and absence of GM-CSF, respectively ($P = 0.75$) (Fig. 1B). Additional studies revealed that both GM-CSF and PFC did not significantly alter PBMC viability on a cell lineage basis (Supplemental Fig. 1A). It was also determined that PFC labeling did not overall impact the GM-CSF-induced activated PBMC phenotype (Supplemental Fig. 1B—E) and thus, GM-CSF-induced PBMC activation may present with enhanced *in vivo* migration of PFC$^+$ PBMC.

GM-CSF promotes *in vivo* migration of PFC$^+$ PBMC

Both 1H and 19F MR imaging was conducted two days after 3 × 10^6 PFC$^+$ PBMC (± GM-CSF) injections into both hind footpads ($n = 4$ donor PBMC, $n = 2$ mice/donor/condition). In total, GM-CSF-treated PFC$^+$ PBMC were detected in 6 of 8 right and 5 of 8 left pLNs (Figs. 2A/B and 3A—C), with the left pLNs having received IL-1β pre-treatment and right pLNs remaining untreated. *In vivo* PFC$^+$ PBMC migration is represented by anatomical/19F MR composite images pseudocoloured using a ''hot-iron'' color scale (Figs. 2 and 3). Untreated PFC$^+$ PBMC produced detectable 19F signal in 1 of 8 right pLNs and 7 of 8 left pLNs (Figs. 2C/D and 3D—F). For pLNs with detectable 19F signal, the signal was quantified as the number of PFC$^+$ cells. GM-CSF appeared to activate PFC$^+$ PBMC to enhance *in vivo* migration above the 19F MRI signal threshold and thus, permitted consistent detection and quantification of migrated cells. This was in contrast to the results observed for untreated PFC$^+$ PBMC, where pre-treatment of the pLN region with IL-1β was required to increase the migration of PFC$^+$ PBMC in the absence of GM-CSF above the 19F MR detection threshold.

Characterization of pLN migration-competent PFC$^+$ PBMC

Successful *in vivo* 19F MRI detection and quantification of PFC$^+$ PBMC (Figs. 2 and 3) raised questions pertaining to the cell lineage composition of pLN-migrated PFC$^+$ PBMC and how this composition compares to pLN-migrated UL PBMC. To address these questions, the donor-specific cell lineage composition of bulk PBMC was determined, followed by negative enrichment to isolate CD3$^+$ T cells (Fig. 4A), CD19$^+$CD20$^+$ B cells (Fig. 4B) and CD14$^+$/CD16$^+$ monocytes (Fig. 4C) to > 95% purity. Each lineage was *ex vivo* cultured with GM-CSF and labeled with PFC or remained UL. Two days later, each lineage (± PFC) was further labeled with a unique membrane-intercalating fluorophore for *in vivo* lineage differentiation (Fig. 4D—F). UL and PFC$^+$ lineages were similarly labeled and to > 99% compared to non-fluorescent lineage-matched cells (Fig. 4D—F). No significant viability differences between pre-injection UL and PFC$^+$ lineages were noted for all lineages (data not shown).

Fluorescent cell lineages were then recombined to closely resemble donor-specific lineage composition and formulated into 3 × 10^6 UL or PFC$^+$ triple-fluorescent left and right hind footpad injections, respectively. The mean cell lineage composition was 52.4 ± 22.2 [SD] % T cells, 16.4 ± 18.1 [SD] % B cells and 31.2 ± 7.8 [SD] % monocytes for all PBMC products ($n = 3$ donors). Two days after adoptive transfer, all cell lineages were present in the central regions of pLN cryosections for both UL (Fig. 4G) and PFC$^+$ (Fig. 4H) triple-fluorescent injection formulations.

Ideally, PFC should label all cells without selectively affecting specific lineages or sub-populations. Therefore, we sought to quantify and compare LN-migrated PFC$^+$ and UL PBMC in a separate experiment. GM-CSF-activated PBMC were cultured as described above to generate UL PBMC and PFC$^+$ PBMC for injection into the left and right hind footpad, respectively. Pre-injection lineage analysis revealed no significant difference in the percentage of CD3$^+$ T cells, CD20$^+$ B cells and CD14$^+$ monocytes between UL and PFC$^+$ conditions (Supplemental Fig. 2A—C). Two days later, single cell suspensions of excised pLNs were subject to flow cytometric analysis to identify human CD45$^+$ cells (Supplemental Fig. 2D). UL and PFC$^+$ injection conditions did not significantly differ with respect to the mean percentage of pLN-migrated human CD45$^+$ cells (UL: 0.85 ± 0.48 [SD] % vs. PFC$^+$: 0.94 ± 0.95 [SD] %; $P = 0.75$) (Fig. 4I), as well as the mean percentage of pLN-migrated CD3$^+$ T cells (UL: 72.2 ± 18.7 [SD] % vs. PFC$^+$: 79.0 ± 16.2%; $P = 0.27$) (Fig. 4J), CD20$^+$ B cells (UL: 11.9 ± 9.1 [SD] % vs. PFC$^+$: 11.7 ± 10.4 [SD] %; $P = 0.96$) (Fig. 4K) and CD14$^+$ monocytes (UL: 6.5 ± 5.7 [SD] % vs. PFC$^+$: 4.4 ± 5.3 [SD] %; $P = 0.43$) (Fig. 4L).

Detection of GM-CSF-treated PFC$^+$ PBMC *in vivo* migration with a 3T clinical MRI set-up

To apply our approach from a pre-clinical to a clinical setting, we performed *in vivo* human PFC$^+$ PBMC migration studies under clinical 3T MRI conditions. Cryopreserved PBMC were cultured overnight with GM-CSF (± PFC) to generate GM-CSF-activated PFC$^+$ and UL PBMC. Mean post-thaw human CD45$^+$ PBMC viability was 96.3% (range: 93.8—99.0%)

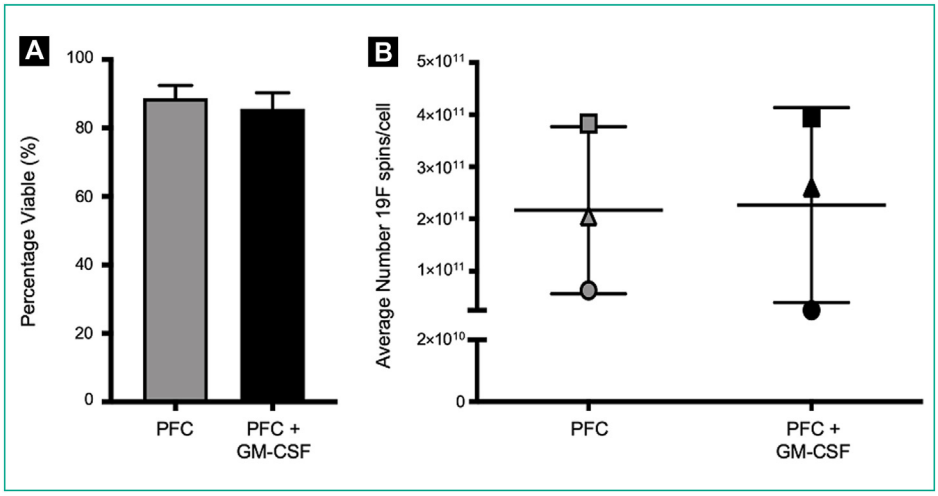

Figure 1. Peripheral blood mononuclear cell (PBMC) viability and perfluorocarbon (PFC) incorporation was unaffected by granulocyte macrophage colony-stimulating factor (GM-CSF). PBMC were labeled with PFC for a total of 48 hours (± GM-CSF addition for the final 24 hours). GM-CSF did not significantly affect PBMC viability (A, 85.7 ± 4.6 [SD] % vs. 88.7 ± 3.7 [SD] %) and average PFC loading (B, 2.27 ± 1.87 [SD] $\times 10^{11}$ vs. 2.17 ± 1.60[SD] $\times 10^{11}$ 19F spins/cell). Data are shown as means ± SD for $n = 3$ independent experiments (paired t-test, $P > 0.05$).

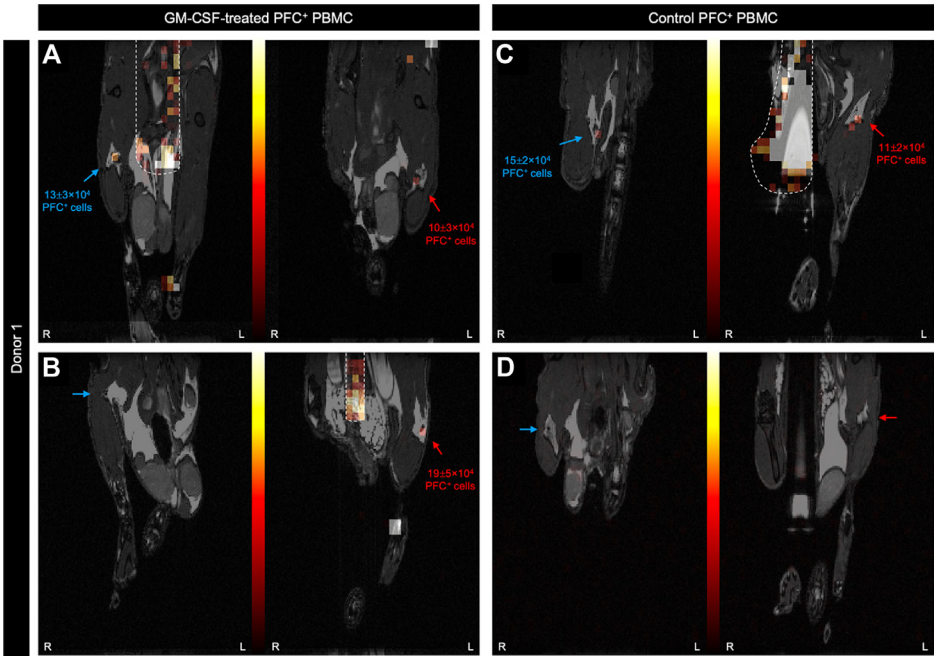

Figure 2. 19F MRI quantification of peripheral blood mononuclear cell (PBMC) *in vivo* migration. Overlaid 1H/19F MR composite images identified right (R, blue arrows) and left (L, red arrows) popliteal lymph nodes (pLNs) from mice that received perfluorocarbon$^+$ (PFC$^+$) granulocyte macrophage colony-stimulating factor (GM-CSF)-treated PBMC injections (A and B) or PFC$^+$ PBMC injections (C and D). 19F signal detected in pLNs is displayed in ''hot-iron'' colour scale and quantified as the number of PFC$^+$ cells (A—D). All left pLN areas received IL-1β pre-treatment (300 ng) three hours before PBMC injection. A reference tube is outlined with a hand-drawn white line and data are presented for $n = 4$ mice injected with $n = 1$ donor PBMC.

(Fig. 5 A) and 92.2% and 89.5% of UL and PFC$^+$ CD45$^+$ PBMC, respectively, remained viable after overnight culture (UL range: 91.6—92.9% and PFC$^+$ range: 87.5—92.4%) (Fig. 5A). PFC labeling did not alter T cell, B cell or monocyte viability (Fig. 5A) or percent composition (Fig. 5B) compared to lineage-matched UL PBMC. Nearly 100% of PBMC incorporated red fluorescent PFC compared to UL PBMC (Fig. 5C), with PFC incorporation measured at $1.15 \pm 0.798 \times 10^{12}$ 19F spins/cell (range: $0.47—2.03 \times 10^{12}$ 19F spins/cell) ($n = 3$ donors) (Fig. 5D). Clinical 3T 1H/19F MR imaging was performed both one day and two days following right and left hind footpad injections ($n = 2—3$ mice/donor). Day 1 (Fig. 5E) and day 2 (Fig. 5F) 1H/19F MRI detected PFC$^+$ cells at the injection site (red arrows), pLNs (orange squares) and iLNs (white brackets). A representative composite 1H/19F three-dimensional MRI video is depicted in Supplemental Movie 1. PFC$^+$ cell migration to pLNs and iLNs (Fig. 5 was quantified on day 1 and day 2 (Fig. 5G) and ranged from

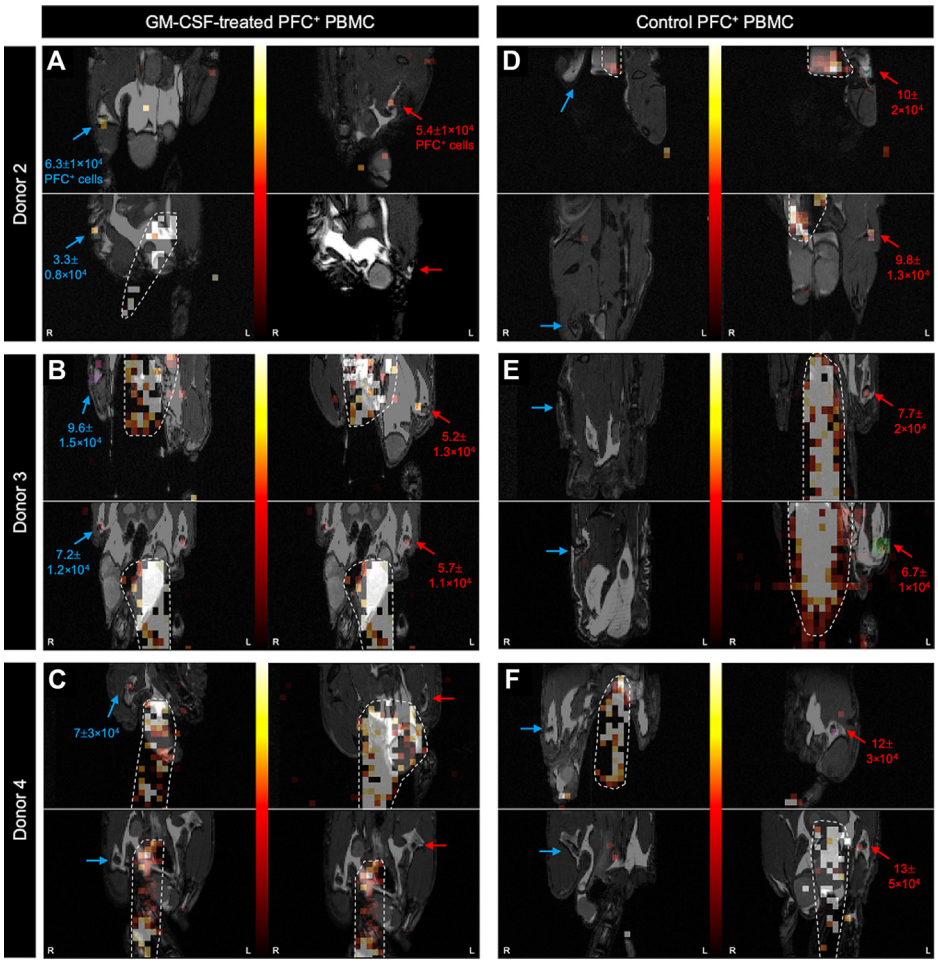

Figure 3. Granulocyte macrophage colony-stimulating factor (GM-CSF)-activation enhanced perfluorocarbon$^+$ (PFC$^+$) peripheral blood mononuclear cell (PBMC) migration to mouse popliteal lymph nodes (pLNs). The adoptive transfer outlined in Fig. 2 was repeated with $n = 3$ donor PBMC. Composite 1H/19F MR images displayed right (R, blue arrows) and left (L, red arrows) pLNs for GM-CSF-treated PFC$^+$ PBMC injected mice (A—C) and similarly for PFC$^+$ PBMC injected mice (D—F). All left pLN areas were pre-treated with IL-1β (300 ng) three hours before PBMC injection. Hand-drawn white lines delineate a reference tube and quantifiable 19F signal in pLNs was shown as number of PFC$^+$ cells. Collectively, data are shown for $n = 4$ PBMC donors ($n = 4$ mice/donor).

0.425—7.08 × 10^5 (day 1) and 0.24—3.41 × 10^5 PFC$^+$ cells (day 2) in the pLNs, while ranges of 2.37—7.40 × 10^5 and 0.278—4.61 × 10^5 PFC$^+$ cells were quantified in the iLNs on day 1 and day 2, respectively. Mice receiving the higher injection dose had migration ranging from 0.115—9.06 × 10^5 (day 1) and 0.608—9.16 × 10^5 PFC$^+$ cells (day 2) in the pLNs and ranging from 0.991—6.91 × 10^5 (day 1) and 0.888—9.89 × 10^5 PFC$^+$ cells (day 2) in iLNs. The detection of human CD45$^+$ cells in single cell suspensions of excised pLNs and iLNs (Fig. 5H) ensured that previously cryopreserved GM-CSF-activated PFC$^+$ PBMC were producing the *in vivo* 19F signal detected using a 3T clinical MR configuration.

Discussion

This study was designed to characterize PFC$^+$ PBMC on a cell lineage basis and determine the compatibility of 19F MRI for *in vivo* cell tracking in conjunction with an established APC-based immunotherapy model [8]. Although previous work has described PFC labeling of all PBMC cell subsets [21], characterization of secondary lymphoid organ-migrated PFC$^+$ PBMC subsets has not been reported. This critical gap in knowledge reduces the accuracy of using *in vivo* imaging as a biomarker of immunotherapeutic effectiveness as each cell lineage within PBMC serves a unique and necessary immunological function.

Prior PFC labeling does not interfere with GM-CSF-mediated APC activation

We have previously optimized conditions for labeling nearly 100% of human PBMC with PFC [21] to improve 19F MRI detection sensitivity. This is an important concept to consider given the added complexity of labeling heterogenous cell populations such as PBMC, which is well represented by a previous study that reported fluorescent PFC uptake in 3.70 ± 0.21 (SD) % of CD3$^+$ cells [26] contained within bulk splenocytes, while 90% of human CD3$^+$ T cells incorporated PFC in homogeneous culture [17]. Cell populations with low cytoplasmic volume such as B and T lymphocytes that have proven difficult to label with contrast agents in the past [27,28] efficiently incorporated PFC under our optimized culture conditions.

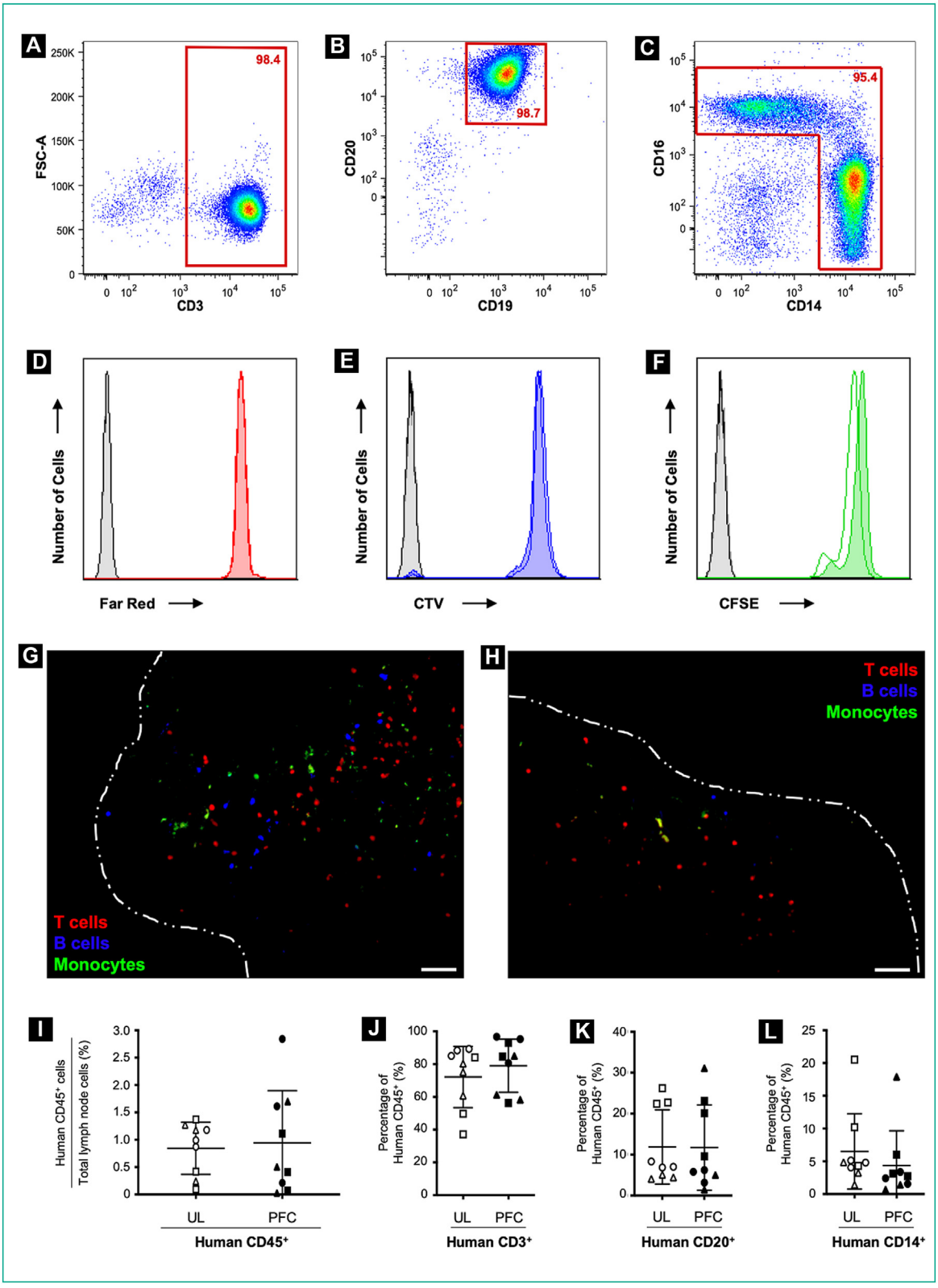

Figure 4. All three main peripheral blood mononuclear cell (PBMC) cell lineages are *in vivo* popliteal lymph node (pLN) migration-competent. Enriched $CD3^+$ T cell (A), $CD19^+CD20^+$ B cell (B) and $CD14^+/CD16^+$ monocyte (C) lineages were cultured for 48 hours (± perfluorocarbon [PFC]), with granulocyte macrophage colony-stimulating factor (GM-CSF) added for the final 24 hours. Nearly 100% of unlabeled (UL) (closed histograms) and PFC^+ (open histograms) T cells fluoresced Far Red^+ (D), B cells CTV^+ (E) and monocytes $CFSE^+$ (F) compared to non-fluorescent UL and PFC^+ controls (D—F, closed and open grey histograms, respectively). Recombined triple-fluorescent PBMC were formulated into UL and PFC^+ hind footpad injections and two days later, excised pLNs contained all 3 cell lineages for both UL and PFC^+ PBMC, respectively (G and H, scale bars = 50 μm and white lines outlined pLNs at 100 × magnification). Separately, pLN were

We next assessed PFC labeling of PBMC in conjunction with GM-CSF addition to culture. PBMC were labeled with PFC prior to GM-CSF addition to take advantage of the impressive PFC uptake by APC within PBMC when in an unactivated state. Efficient PFC uptake occurred before GM-CSF-induced APC activation. APC activation demonstrated here may coincide with decreased antigen uptake and presumably, decreased PFC uptake as has been reported for DC [10,21,29]. PBMC viability remained consistently high (> 85%) throughout culture, which was expected considering PFC is comprised of an inert emulsion stabilized by surfactant and is retained within the viable cell populations of interest [18,30]. Interparticipant differences in PFC incorporation were attributed to the wide range of cell lineage proportions within PBMC that range from 18.7—71.4% for T cells, 3.36—27.7% for B cells and 7.14—45.3% for monocytes [22] and although unavoidable, this must be considered with respect to 19F MRI sensitivity.

Each cell lineage serves a specific and necessary immunological purpose and thus, it was imperative to demonstrate that PFC did not disproportionately affect the viability, phenotype and function of specific cell lineages. PBMC phenotype was assessed both by frequency and intensity of expression (MFI) for activation, co-stimulation and migration markers required for APC to function as adjuvants in an immunotherapeutic setting. For all culture conditions, both B cells and myeloid cells expressed CD40, CD86 and CD54. Nearly all UL and PFC$^+$ B cells were CD40$^+$, which is critical for induction of T_H1-mediated and T_H2-/humoral-mediated immune response through interaction with CD154 on CD4$^+$ T_H cells [9,29]. In mCRPC patients that received Sipuleucel-T (Provenge®), from two weeks up until 6 months, IgG responses to PAP and other non-targeted TAA arising from antigen spread (prostate-specific antigen and LGALS3/Galectin 3) were associated with prolonged overall survival [31]. Furthermore, CD54$^+$ APC that co-express CD40, CD86 and human leukocyte antigen (HLA)-A, B, C and HLA-DR can present TAA alongside appropriate co-stimulatory signalling necessary to induce both TAA-specific CD8$^+$ and CD4$^+$ T cells [32—34]. GM-CSF moderately induced APC to express an activated phenotype that included significant upregulation of CD86 on B cells and significant upregulation of CD86 and CD54 on myeloid cells, suggesting that GM-CSF is biologically active in our experimental system. We also believe that the CD54$^+$ myeloid cells reported here closely mimic the large CD54$^+$ APC within Sipuleucel-T (Provenge®) cell products [12].

19F MRI detection and quantification of PFC$^+$ PBMC *in vivo* migration at 9.4T

We next sought to determine if 19F MRI was a suitable imaging modality to detect differences in PFC$^+$ PBMC *in vivo* migration associated with GM-CSF inclusion in culture. Pre-treatment of the draining pLN with IL-1β before adoptive cell transfer was also included to improve *in vivo* PFC$^+$ PBMC migration as a means of enhancing immunotherapeutic effectiveness [15,23,35]. GM-CSF-activation of PFC$^+$ PBMC and IL-1β pre-treatment of recipient mice did not function synergistically to improve PFC$^+$ PBMC migration to the pLN. However, IL-1β pre-treatment appeared to improve migration above the 19F MRI detection threshold for PFC$^+$ PBMC not activated with GM-CSF.

GM-CSF-activated PFC$^+$ PBMC exhibited an improved capacity to reach the draining pLN that permitted consistent detection and quantification using 19F MRI. GM-CSF did not affect expression of the migration marker CCR7 as assessed here; however, GM-CSF has been shown to modulate the expression other chemokine receptors such as CCR5 and CXCR4 that mediate cell migration to, and retention within, secondary lymphoid organs [36,37]. Alternatively, GM-CSF activation of PFC$^+$ PBMC, through interaction with its cognate receptor CD116, induces CD54 upregulation. CD54, alternatively known as intracellular adhesion molecule 1 (ICAM-1), stabilizes the immunological synapse between APC and T cell via interaction with lymphocyte function-associated antigen 1 [11,38,39]. We have previously shown *in vitro* that both PFC$^+$ and control UL APC are equally capable of inducing allogeneic CD4$^+$ and CD8$^+$ T cell proliferation in a human mixed lymphocyte reaction and that PFC$^+$ and control UL mouse bone marrow-derived DC equivalently stimulate an antigen-specific CD8$^+$ T cell response in immunocompetent C57BL/6 mice [19,21]. Therefore, we predict that GM-CSF activation of PBMC promotes APC retention in the LN, thereby fostering immunologically successful interactions with T cells, and resulting in an improved immunogenicity of the subsequent antigen-specific immune response [40]. Moreover, activated APC within PBMC can contribute to a positive feedback loop via IL-12 and IFNγ release. These pro-inflammatory cytokines activate T and natural killer cells to release TNFα and additional IFNγ that, in turn, can then activate APC in a paracrine manner [34,41]. With this outlined mechanism, GM-CSF-induced APC activation and positive feedback pro-inflammatory cytokine secretion could present as increased PFC$^+$ PBMC in the pLN as quantified by 19F MRI in this study.

Characterization of pLN-migrated PFC$^+$ cells

The question arose following successful PFC$^+$ PBMC detection in pLNs with 19F MRI as to which cell lineages were contributing to the measured 19F signal. Until this point, it was assumed that the relative cell lineage proportions in pre-injection PFC$^+$ PBMC were similar to the LN-migrated cell lineage proportions. Secondly, from an

digested 48 hours following hind footpad injection of GM-CSF-treated non-fluorescent UL and PFC$^+$ PBMC to identify pLN-migrated human CD45$^+$ using flow cytometry (I, white and black data points, respectively). No significant differences in quantified pLN-migrated human CD3$^+$ T cells (J), human CD20$^+$ B cells (K) and human CD14$^+$ monocytes (L) were noted between UL and PFC$^+$ injection conditions. Data are shown for $n = 3$ donor PBMC ($n = 4$—5 mice/donor) (A—H). For panels I—L, data was expressed as means ± SD for $n = 3$ donor PBMC ($n = 3$ mice/donor) (I—L, $P > 0.05$).

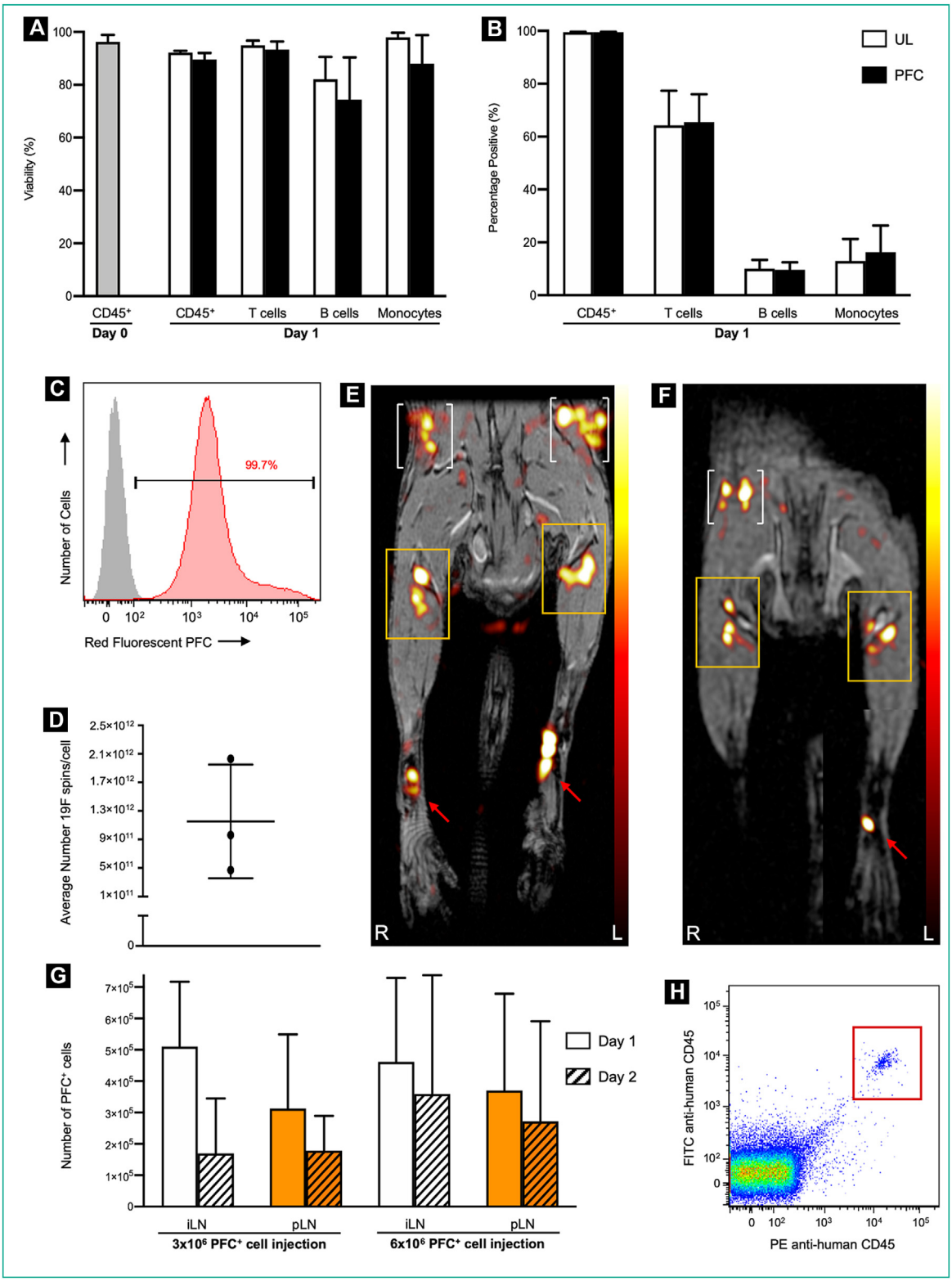

Figure 5. Clinical 3T MRI detection of cryopreserved perfluorocarbon$^+$ (PFC$^+$) peripheral blood mononuclear cell (PBMC) migration to draining mouse lymph nodes (LNs). Post-thaw CD45$^+$ PBMC viability was $96.3 \pm 2.6\%$ (A, day 0) and remained high after culture with granulocyte macrophage colony-stimulating factor (GM-CSF) for both unlabeled (UL) and PFC$^+$ total CD45$^+$ PBMC, as well as for T cell, B cell and monocyte lineages (A, day 1, white and black bars, respectively). PFC incorporation did not alter cell lineage composition compared to UL PBMC (B, day 1, white and black bars, respectively). Nearly 100% of PBMC incorporated red fluorescent PFC (C, red histogram, UL PBMC gray histogram) and the mean PFC loading was $1.15 \pm 0.798 \times 10^{12}$ 19F spins/cell for $n = 3$ donor PBMC (D). Mice ($n = 2-3$/donor) that received 3×10^6 and 6×10^6 PFC$^+$ PBMC right (R) and (L) hind footpad injections, respectively, had 19F signal detected at both 24 hours (E) and 48 hours (F) at the footpad (red arrows), popliteal LNs (pLNs, orange boxes) and inguinal LNs (iLN, white brackets). Quantified 19F

immunological perspective, defining and quantifying which cell lineages reach the LN is important due to the defined functions each lineage serves in secondary lymphoid organs.

By labeling enriched GM-CSF-treated $CD3^+$ T cells, $CD19^+CD20^+$ B cells and $CD14^+/CD16^+$ monocytes with unique fluorophores we were not only able to assess *in vivo* migration of PBMC on a per lineage basis but also compare this migration between UL and PFC^+ conditions. A slight decrease in CFSE fluorescence was noted in PFC^+ monocytes compared to UL monocytes and is most likely a result of monocytes incorporating the largest amount of PFC. Even so, the fluorescence from CFSE-labeled PFC^+ monocytes is multiple log folds higher than for $CFSE^{Neg}$ monocytes, rendering them easily distinguishable from non-fluorescent surrounding cells. PFC labeling does not interfere with *in vivo* migration as all three main lineages from both UL and PFC^+ PBMC were detected in the pLN, with the majority of cells penetrating into central paracortical and follicular regions of this organ. The observed penetrance of $CFSE^+$ monocytes into central LN regions suggests that such monocytes differentiated into moDC due to GM-CSF addition to culture, further confirming GM-CSF bioactivity in our cultures [42]. Considering that the monocyte to moDC transition and subsequent maturation is dynamic and continues throughout *in vivo* migration to the LN the slight differences in APC activation state between PFC^+ and UL conditions prior to injection may be restored or modified upon reaching the pLN. Further phenotyping for HLA-DR and CD11c upregulation, cytokine secretion profiles, as well as quantification of the ensuing TAA-specific immune response would be required to fully answer this hypothesis. The implications of monocyte to DC differentiation are promising given that DC are professional APC capable of launching long-term potent *de novo* immune responses through interaction and activation of naïve $CD4^+$ and $CD8^+$ T cells [32,35] in paracortical LN regions.

The previous experiment required extensive *ex vivo* manipulation and lineage enrichment, which have the potential to alter cell activation status [43]. To accurately quantify *in vivo* migration, we conducted a separate experiment void of numerous *ex vivo* manipulation steps. Flow cytometric analysis of LN cell suspensions revealed that PFC labeling of PBMC did not interfere with the number of pLN-migrated human $CD45^+$ compared to UL PBMC and that PFC labeling did not disproportionately affect one cell lineage over another. Additionally, the composition of pLN-migrated human $CD45^+$ cells closely resembled the pre-injection PBMC composition. Taken together, this data confirms our previous assumption of PFC^+ PBMC composition remaining constant after *in vivo* migration holds true and therefore, quantification of *in vivo* PBMC migration using 19F MRI stands as an accurate and non-invasive biomarker of APC-based immunotherapeutic effectiveness.

Cryopreserved PFC^+ PBMC are lymph node migration-competent and detectable using a clinical 3T 19F MRI configuration

We transitioned from pre-clinical (9.4T) to our current clinical (3T) MRI set-up that included a hardware upgrade for dual nuclei (1H/19F) detection and employed a highly sensitive surface coil to combat the lower sensitivity associated with 19F cellular MRI. SNR was improved through averaging alongside aforementioned optimized PFC labeling conditions to render highly specific ''hot-spot'' detection of 19F MR signal possible in a clinical setting [18,20,21,27,44]. Clinical tracking of PFC^+ DC has been described and we have outlined a Good Manufacturing Practice-compliant protocol that yields *in vivo* LN migration-competent PFC^+ PBMC detected at 9.4T [21,45]. We then shortened our *ex vivo* protocol and used cryopreserved PBMC to test the robustness of 19F MRI therapeutic cell tracking in a clinical setting.

With a shortened protocol for PFC labeling and GM-CSF addition to culture, nearly 100% of previously cryopreserved PBMC incorporated PFC similarly to fresh PBMC. Neither cryopreservation nor PFC labeling reduced PBMC viability in our hands, which is immunologically important given that apoptotic APC can lead to induction of tolerance in a cancer immunotherapy model [9]. Purposeful migration of PFC^+ PBMC to draining pLN and downstream iLNs demonstrated that cryopreservation does not alter PBMC *in vivo* migration. Together with positive cell surface staining for human $CD45^+$ cells in excised LN cell suspensions shown by our group [21], we are confident that the originally-injected PFC^+ human PBMC are the source of detected *in vivo* 19F MR signal. This also indicates that the majority of LN-migrated human $CD45^+$ cells remain intact and viable, and thus, false positive signal due to apoptotic human PFC^+ cell engulfment by mouse resident phagocytes is not confounding our observed results. Finally, longitudinal detection of PFC^+ PBMC in pLNs and iLNs both one day and two days after adoptive transfer provides further evidence supporting our proposed mechanism of GM-CSF-induced migration to and retention of activated APC within secondary lymphoid organs.

Conclusion

In conclusion, this study further details the suitability of 19F MRI as a non-invasive imaging modality to predict APC-based vaccine immunotherapy effectiveness that is robust enough to handle unavoidable interpatient differences in PBMC composition yet sensitive enough to detect subtle differences in *in vivo* PBMC migration as a result of APC activation using an established method [8]. What started as a drawback — labeling a heterogeneous cell population with PFC — resulted in the successful labeling of other PBMC cell lineages with distinct functions that play key roles in other current and emerging immunotherapies.

signal was summarized in (G). Human $CD45^+$ PFC^+ PBMC detected in pLN cell suspensions (H, red box) confirmed that originally-injected PFC^+ PBMC are the source of *in vivo* 19F signal.

Human and animal rights

The authors declare that the work described has not involved experimentation on humans or animals.

Informed consent and patient details

The authors declare that they obtained a written informed consent from the patients and/or volunteers included in the article and that this report does not contain any personal information that could lead to their identification.

Funding

This research was supported by grants from the Ontario Institute for Cancer Research Smarter Imaging Program [Grant Number R4174A19], Foundation Grant for Prostate Cancer Research [Grant Number R2417A21] and Dendreon Corporation [Proof of Concept Project, Grant Number R2417A20].

Authors' contributions

Corby Fink, PhD: conceptualization, data curation, formal analysis, investigation, methodology, writing and subsequent editing of original draft. Michael Smith, MSc: data curation, formal analysis, investigation and editing of draft. Olivia C. Sehl, BSc: data curation, formal analysis and investigational aspects related to 3T MRI, writing — review and editing. Jeffrey M. Gaudet, PhD: conceptualization, data curation, formal analysis, investigation, methodology with respect to 19F MRI, writing — review and editing. Thomas Craig Meagher, PhD: conceptualization, writing — review and editing. Nadeem A. Sheikh, PhD: conceptualization and editing. Jimmy D. Dikeakos, PhD: supervision, writing — review and editing. Michael J. Rieder, MD, PhD: methodology and editing. Paula J. Foster, PhD: conceptualization, funding acquisition, methodology for MRI, project administration, supervision, writing — review and editing. Gregory A. Dekaban, PhD: conceptualization, funding acquisition, methodology, project administration, supervision, writing — review and editing.

Acknowledgements

The authors thank Jason Chinn for his technical expertise.

Disclosure of interest

The authors from the Robarts Research Institute and University of Western Ontario have no competing interests with the exception of Jeffrey M. Gaudet (Magnetic Insight, Inc.). Relationships are declared for Thomas C. Meagher (Dendreon Corporation and Regeneron Pharmaceuticals, Inc.) and Nadeem A. Sheikh (Dendreon Corporation).

Appendix A. Supplementary data

Supplementary data associated with this article can be found, in the online version, at https://doi.org/10.1016/j.diii.2020.02.004.

Références

[1] Sharma P, Hu-Lieskovan S, Wargo JA, Ribas A. Primary, adaptive, and acquired resistance to cancer immunotherapy. Cell 2017;168:707—23.
[2] Baitsch L, Baumgaertner P, Devevre E, Raghav SK, Legat A, Barba L, et al. Exhaustion of tumor-specific CD8(+) T cells in metastases from melanoma patients. J Clin Invest 2011;121:2350—60.
[3] Sabado RL, Balan S, Bhardwaj N. Dendritic cell-based immunotherapy. Cell Res 2017;27:74—95.
[4] Schreibelt G, Benitez-Ribas D, Schuurhuis D, Lambeck AJ, van Hout-Kuijer M, Schaft N, et al. Commonly used prophylactic vaccines as an alternative for synthetically produced TLR ligands to mature monocyte-derived dendritic cells. Blood 2010;116:564—74.
[5] Scheid E, Major P, Bergeron A, Finn OJ, Salter RD, Eady R, et al. Tn-MUC1 DC vaccination of Rhesus macaques and a phase I/II trial in patients with nonmetastatic castrate-resistant prostate cancer. Cancer Immunol Res 2016;4:881—92.
[6] Atilla E, Kilic P, Gurman G. Cellular therapies: day by day, all the way. Transfus Apher Sci 2018;57:187—96.
[7] Sakhno LV, Shevela EY, Tikhonova MA, Ostanin AA, Chernykh ER. The phenotypic and functional features of human M2 macrophages generated under low serum conditions. Scand J Immunol 2016;83:151—9.
[8] Small EJ, Schellhammer PF, Higano CS, Redfern CH, Nemunaitis JJ, Valone FH, et al. Placebo-controlled phase III trial of immunologic therapy with sipuleucel-T (APC8015) in patients with metastatic, asymptomatic hormone refractory prostate cancer. J Clin Oncol 2006;24:3089—94.
[9] Waldmann TA. Cytokines in cancer immunotherapy. Cold Spring Harb Perspect Biol 2018;10:a028472.
[10] Benteyn D, Heirman C, Bonehill A, Thielemans K, Breckpot K. mRNA-based dendritic cell vaccines. Expert Rev Vaccines 2015;14:161—76.
[11] Sheikh NA, Jones LA. CD54 is a surrogate marker of antigen presenting cell activation. Cancer Immunol Immunother 2008;57:1381—90.
[12] Kantoff PW, Higano CS, Shore ND, Berger ER, Small EJ, Penson DF, et al. Sipuleucel-T immunotherapy for castration-resistant prostate cancer. N Engl J Med 2010;363:411—22.
[13] Boettcher AN, Usman A, Morgans A, VanderWeele DJ, Sosman J, Wu JD. Past, current, and future of immunotherapies for prostate cancer. Front Oncol 2019;9:884.
[14] Forster R, Braun A, Worbs T. Lymph node homing of T cells and dendritic cells via afferent lymphatics. Trends Immunol 2012;33:271—80.
[15] Martin-Fontecha A, Sebastiani S, Hopken UE, Uguccioni M, Lipp M, Lanzavecchia A, et al. Regulation of dendritic cell migration to the draining lymph node: impact on T lymphocyte traffic and priming. J Exp Med 2003;198:615—21.
[16] Wang B, Sun C, Wang S, Shang N, Shangguan J, Figini M, et al. Mouse dendritic cell migration in abdominal lymph nodes by intraperitoneal administration. Am J Transl Res 2018;10:2859—67.
[17] O'Hanlon CF, Fedczyna T, Eaker S, Shingleton WD, Helfer BM. Integrating a 19F MRI tracer agent into the clinical scale manufacturing of a T-cell immunotherapy. Contrast Media Mol Imaging 2017;2017 [9548478].

[18] Chapelin F, Capitini CM, Ahrens ET. Fluorine-19 MRI for detection and quantification of immune cell therapy for cancer. J Immunother Cancer 2018;6:105.
[19] Fink C, Smith M, Gaudet JM, Makela A, Foster PJ, Dekaban GA. Fluorine-19 cellular MRI detection of *in vivo* dendritic cell migration and subsequent induction of tumor antigen-specific immunotherapeutic response. Mol Imaging Biol 2019, http://dx.doi.org/10.1007/s11307-019-01393-8.
[20] Gaudet JM, Hamilton AM, Chen Y, Fox MS, Foster PJ. Application of dual (19) F and iron cellular MRI agents to track the infiltration of immune cells to the site of a rejected stem cell transplant. Magn Reson Med 2017;78:713—20.
[21] Fink C, Gaudet JM, Fox MS, Bhatt S, Viswanathan S, Smith M, et al. ^{19}F-perfluorocarbon-labeled human peripheral blood mononuclear cells can be detected *in vivo* using clinical MRI parameters in a therapeutic cell setting. Sci Rep 2018;8:590.
[22] Burel JG, Qian Y, Lindestam Arlehamn C, Weiskopf D, Zapardiel-Gonzalo J, Taplitz R, et al. An integrated workflow to assess technical and biological variability of cell population frequencies in human peripheral blood by flow cytometry. J Immunol 2017;198:1748—58.
[23] Vuylsteke RJ, Molenkamp BG, Gietema HA, van Leeuwen PA, Wijnands PG, Vos W, et al. Local administration of granulocyte/macrophage colony-stimulating factor increases the number and activation state of dendritic cells in the sentinel lymph node of early-stage melanoma. Cancer Res 2004;64:8456—60.
[24] Gaudet JM, Ribot EJ, Chen Y, Gilbert KM, Foster PJ. Tracking the fate of stem cell implants with fluorine-19 MRI. PLoS One 2015;10:e0118544.
[25] Srinivas M, Morel PA, Ernst LA, Laidlaw DH, Ahrens ET. Fluorine-19 MRI for visualization and quantification of cell migration in a diabetes model. Magn Reson Med 2007;58:725—34.
[26] Gonzales C, Yoshihara HA, Dilek N, Leignadier J, Irving M, Mieville P, et al. *In vivo* detection and tracking of T cells in various organs in a melanoma tumor model by ^{19}F-Fluorine MRS/MRI. PLoS One 2016;11:e0164557.
[27] Dekaban GA, Hamilton AM, Fink CA, Au B, de Chickera SN, Ribot EJ, et al. Tracking and evaluation of dendritic cell migration by cellular magnetic resonance imaging. WIREs Nanomed Nanobi 2013;5:469—83.
[28] Hwang YH, Lee DY. Magnetic resonance imaging using heparin-coated superparamagnetic iron oxide nanoparticles for cell tracking *in vivo*. Quant Imaging Med Surg 2012;2:118—23.
[29] Lopez-Relano J, Martin-Adrados B, Real-Arevalo I, Lozano-Bartolome J, Abos B, Sanchez-Ramon S, et al. Monocyte-derived dendritic cells differentiated in the presence of lenalidomide display a semi-mature phenotype, enhanced phagocytic capacity, and Th1 polarization capability. Front Immunol 2018;9:1328.
[30] Waiczies H, Lepore S, Janitzek N, Hagen U, Seifert F, Ittermann B, et al. Perfluorocarbon particle size influences magnetic resonance signal and immunological properties of dendritic cells. PLoS One 2011;6:e21981.
[31] Guhathakurta D, Sheikh NA, Fan LQ, Kandadi H, Meagher TC, Hall SJ, et al. Humoral immune response against nontargeted tumor antigens after treatment with Sipuleucel-T and its association with improved clinical outcome. Clin Cancer Res 2015;21:3619—30.
[32] Martin K, Schreiner J, Zippelius A. Modulation of APC function and anti-tumor immunity by anti-cancer drugs. Front Immunol 2015;6:501.
[33] Lacher MD, Bauer G, Fury B, Graeve S, Fledderman EL, Petrie TD, et al. SV-BR-1-GM, a clinically effective GM-CSF-secreting breast cancer cell line, expresses an immune signature and directly activates CD4(+) T lymphocytes. Front Immunol 2018;9:776.
[34] Ma DY, Clark EA. The role of CD40 and CD154/CD40L in dendritic cells. Semin Immunol 2009;21:265—72.
[35] Verdijk P, Aarntzen EH, Lesterhuis WJ, Boullart AC, Kok E, van Rossum MM, et al. Limited amounts of dendritic cells migrate into the T-cell area of lymph nodes but have high immune activating potential in melanoma patients. Clin Cancer Res 2009;15:2531—40.
[36] Wimmers F, Schreibelt G, Skold AE, Figdor CG, De Vries IJ. Paradigm shift in dendritic cell-based immunotherapy: from *in vitro* generated monocyte-derived DCs to naturally circulating DC subsets. Front Immunol 2014;5:165.
[37] Iwabuchi R, Ikeno S, Kobayashi-Ishihara M, Takeyama H, Ato M, Tsunetsugu-Yokota Y, et al. Introduction of human Flt3-L and GM-CSF into humanized mice enhances the reconstitution and maturation of myeloid dendritic cells and the development of Foxp3(+)CD4(+) T cells. Front Immunol 2018;9:1042.
[38] Goldstein JIK, Jacobson DJ, Bowers N, Regalia B, Austin K, Yousefi GL, et al. Defective leukocyte GM-CSF receptor (CD116) expression and function in inflammatory bowel disease. Gastroenterology 2011;141:208—16.
[39] Van Seventer GA, Shimizu Y, Horgan KJ, Shaw S. The LFA-1 ligand ICAM-1 provides an important costimulatory signal for T cell receptor-mediated activation of resting T cells. J Immunol 1990;144:4579—86.
[40] Sahin U, Tureci O. Personalized vaccines for cancer immunotherapy. Science 2018;359:1355—60.
[41] Oh E, Oh JE, Hong J, Chung Y, Lee Y, Park KD, et al. Optimized biodegradable polymeric reservoir-mediated local and sustained co-delivery of dendritic cells and oncolytic adenovirus co-expressing IL-12 and GM-CSF for cancer immunotherapy. J Control Release 2017;259:115—27.
[42] Castiello L, Sabatino M, Jin P, Clayberger C, Marincola FM, Krensky AM, et al. Monocyte-derived DC maturation strategies and related pathways: a transcriptional view. Cancer Immunol Immunother 2011;60:457—66.
[43] Guhathakurta D, Sheikh NA, Meagher TC, Letarte S, Trager JB. Applications of systems biology in cancer immunotherapy: from target discovery to biomarkers of clinical outcome. Expert Rev Clin Pharmacol 2013;6:387—401.
[44] Bulte JW, Kraitchman DL. Iron oxide MR contrast agents for molecular and cellular imaging. NMR Biomed 2004;17:484—99.
[45] Ahrens ET, Helfer BM, O'Hanlon CF, Schirda C. Clinical cell therapy imaging using a perfluorocarbon tracer and fluorine-19 MRI. Magn Reson Med 2014;72:1696—701.